15

A Closed-Loop Method for Bio-Impedance Measurement with Application to Four and Two-Electrode Sensor Systems

Alberto Yúfera and Adoración Rueda
Instituto de Microelectrónica de Sevilla (IMS),
Centro Nacional de Microelectrónica (CNM)
University of Seville
Spain

1. Introduction and Motivation

Impedance is a useful parameter for determining the properties of matter. Today, many research goals are focused to measure the impedance of biological samples. Several are the major benefits of measuring impedances in medical and biological environment: first, most biological parameters and processes as glucose concentration (Beach, 2005), tissue impedance evolution (Yúfera et al., 2005), cell-growth tax (Huang, 2004), toxicological analysis (Radke, 2004), bacterial detection (Borkholder, 1998), etc, can be monitored using its impedance as marker. Second, the bio-impedance measurement is a non-invasive technique and third, it represents a relatively cheap technique at labs. Electrical Impedance Tomography (EIT) in bodies (Holder, 2005), and Impedance Spectroscopy (IS) of cell cultures (Giaever, 1993) are two examples of the impedance utility for measuring biological and medical parameters.

For the problem of measuring any given impedance Z_x, with magnitude Z_{xo} and phase ϕ, several methods have been reported. Commonly, these methods require excitation and processing circuits. Excitation is usually done with AC current sources, while processing steps are based on coherent demodulation principle (Ackmann, 1984) or synchronous sampling (Pallas et al., 1993), leading to excellent results. In both, processing circuits must be synchronized with input signals, as a requirement for the technique to work, obtaining the best noise performance when proper filter functions (HP and LP) are incorporated. Block diagrams for both are illustrated in Figures 1 (a) and (b) respectively. The main drawback for the Ackmann method is that the separated channels for in-phase and quadrature components must be matched to avoid large phase errors. Synchronous sampling proposed by Pallas avoids two channels and demodulation, by selecting accurate sampling times, and adding a high pass filter in the signal path to prevent low-frequency noise and sampler interferences. These measurement principles work as feed-forward systems: the signal generated on Z_x is amplified and then processed. In general, for an impedance measurement

process based on electrodes, one of the main drawbacks on excitation circuit design is imposed by the need of using electrodes and its electrical performance, which is frequency dependent, having low frequency impedance values in the MΩ range. Also, applied voltage to electrodes must be amplitude limited to guarantee its correct biasing region, generally some tens of mV.

This work presents a Closed-loop method for Bio-Impedance Measurement (CBIM) based on the application of AC voltage signals, with constant amplitude, to impedance under test (ZUT). The proposed method can be applied to electrode-based sensor systems, solving the electrode frequency dependence problem by including electrode electrical models in the circuit design equations, in such a way that enables the circuit derived for measuring impedance of specific biological samples. In this chapter we develop the idea of using feedback for measuring impedances and propose the circuits employed for adapting the excitation signal to ZUT and electrodes. The CBIM method allows the possibility of considering the electrode performance at the initial phase of an experiment where the electrode characteristics (size, material, etc.) are selected depending on the biological material to be tested and the sensitivity required by the experiment. The magnitude and phase impedance are obtained directly from the proposed circuits using easy to acquire signals: a DC voltage, for magnitude, and a duty cycle of a digital signal, for phase. The proposed method is implemented with CMOS circuits, showing through electrical simulations the correct performance for a wide frequency and load ranges. The possibility of integrated CMOS electrodes also opens the door to fully lab-on-chip systems. The CBIM technique represents an alternative method for measuring, using two and four electrode setups, in techniques such as Electric Cell-substrate Impedance Spectroscopy (ECIS) and Electrical Impedance Tomography (EIT), respectively, and some examples are developed in the chapter.

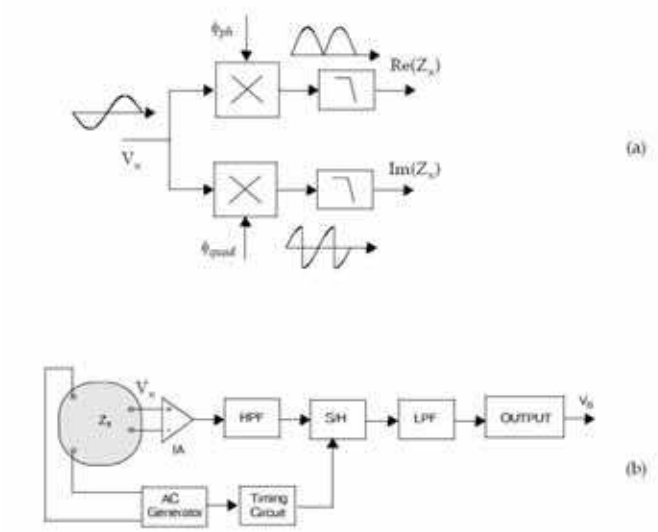

Fig. 1. (a) Synchronous demodulation. (b) Synchornous sampling.

The proposed content of the chapter is the following. The second section presents the CBIM method, its main blocks, system design equations and limitations in terms of its functional

block parameters and the system specifications. The third section describes the CMOS circuits implementing the system: topology, design equations and performance limitations (design issues) for each circuit and related to the global system. The fourth section is dedicated to electrical simulation exercises of some examples to validate the proposed method. The fifth section relies on the CBIM application on a four-electrode system. Real electrode models are incorporated to the system design process and simulations. Finally, in the sixth section, a two-electrode system for cell culture applications is analysed from two perspectives: first, considering a single-cell location problem, and second, dealing with a bi-dimensional array of sensors (electrodes). This approach allows the achievement of an alternative technique for real-time monitoring and imaging cell cultures. An example of this approach is included.

2. Proposed Closed-Loop Method for Bio-Impedance Measurement

A general process for measuring a given impedance Z_x (with magnitude Z_{xo} and phase ϕ) is based on the application of an input signal (current or voltage) to create a response signal (voltage or current) and then, to extract from this its components (real and imaginary parts or magnitude and phase). This concept is illustrated on Fig. 2(a), with a current source i_x as excitation signal. This is generally an AC signal of a given amplitude (i_{xo}) and frequency (ω). Z_s considers the path resistance from source to load, and usually includes parasitic resistances from the set-up and the electrode impedance. The latter has a large magnitude and frequency dependency in the range of interest. Signal $V_x(t)$ is the voltage response obtained by applying $i_x(t)$ in series with the impedance under test (ZUT). The amplified voltage, $V_o(t)$, is processed to obtain the impedance components. Excitation and processing are usually performed by different circuits, though connected by synchronized signals.
The Z_x impedance can also be measured with a feedback system, as illustrated in Fig. 2(b), by introducing a new block, ZF. The signal excitation will depend on the amplifier output and hence on the ZUT. This idea is used to design an alternative method for impedance measurement using the feedback principle. The targets imposed to ZF feedback block are:

1) to generate the i_x excitation signal.
2) to provide the measurement of magnitude and phase.

Meanwhile, a main specification is set: *the voltage amplitude at impedance under test, V_x, must be constant.* This condition is known as the potentiostat (Pstat) condition for impedance measurement and means to setting constant and limited the voltage amplitude V_{xo} "seen" by the ZUT (Yúfera et al., 2008). From the system in Fig. 2b, voltage at Z_x has a constant amplitude, hence changes in magnitude Z_{xo} must modify the amplitude of the applied current, i_{xo}. The current i_x fits its amplitude to preserve constant the voltage amplitude on Z_x and holds the information about the Z_x magnitude. This current must be generated by the ZF block. As a consequence, the amplitude at the instrumentation amplifier (IA) output voltage is constant. The discrimination between signals with different phases are observed in terms of its delays ϕ in the voltage,

$$V_o = V_o(Z_x) = V_{ia} \sin(\omega t + \phi) \quad (1)$$

being α_{ia} the instrumentation amplifier gain.

In conclusion, when feedback is applied in a system for measuring a given impedance in Pstat conditions (as aforementioned), the amplitude of the excitation current, i_{xo}, has the information about the magnitude of the ZUT, while its phase shift, ϕ, must be extracted from the constant amplitude signal in eq. (1). The measurement strategy for Z_x can benefit from the resulting conditions. A change from the method proposed in (Pallas et al., 1993) is that the magnitude and phase can be obtained directly from two different signals, being possible to separate circuit optimization tasks for both signals.

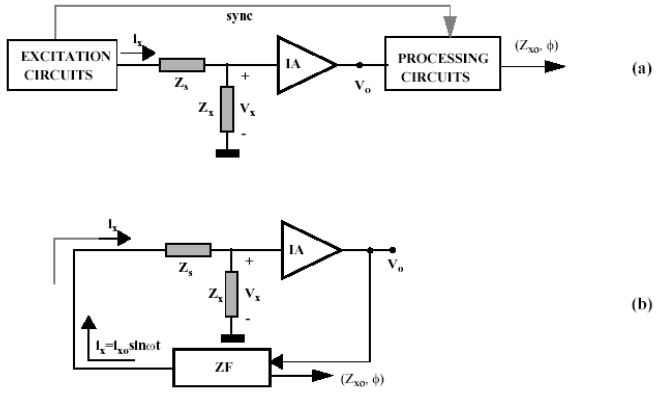

Fig. 2. (a) Basic concept for measuring the Z_{xo} and ϕ components of Z_x. (b) Proposed idea for measuring Z_x using a feedback system.

3. Basic Circuit Blocks

3.1 System Specifications

For the measurement of the impedance magnitude, Z_{xo}, it will be considered that the excitation signal is an AC current, with amplitude i_{xo} and frequency ω. The proposed circuit block diagram for ZF is shown in Fig.3. Three main components are included: an AC-to-DC converter or rectifier, an error amplifier, and a current oscillator with programmable output current amplitude. The rectifier works as a full wave peak-detector, sensing the biggest (lowest) amplitude of V_o. This functionality allows to control the output voltage swing at the instrumentation voltage acting as an envelop detector. Its result is a DC voltage, V_{dc}, with low rippley, directly proportional to the amplitude of the instrumentation amplifier output voltage, and with an α_{dc} gain ($V_{dc}=\alpha_{dc}.\alpha_{ia}V_{xo}$). The error amplifier (EA) will compare the DC signal with a voltage reference, V_{ref}, giving its amplified difference: $V_m=\alpha_{ea}.(V_{dc}-V_{ref})$. The voltage V_{ref} represents the constant voltage reference required to work in the Pstat mode, and can be interpreted as a calibration constant. The full rectifier output voltage must approach as near to V_{ref} as possible. The current oscillator generates the AC current to excite the ZUT. It is composed by a external AC voltage source, V_s, an operational transconductance amplifier (OTA), with g_m transconductance, and a voltage multiplier with K constant. The voltage source V_s, $V_{so}.\sin\omega t$, is multiplied by V_m, and then current converted with the OTA. The equivalent transconductance from the magnitude voltage, V_m, to the excitation current, i_x, is called G_m and will depend on the AC voltage amplitude, V_{so}, the K

multiplier constant and the g_m of the OTA. The equivalent transconductance for the current oscillator is defined as $G_m = g_m.V_{so}.K$. A simple analysis of the full system gives the following expression for the voltage amplitude at the ZUT,

$$V_{xo} = \frac{Z_{xo}.G_m.\alpha_{ea}.V_{ref}}{1 + Z_{xo}.G_m.\alpha_{ea}.\alpha_{ia}.\alpha_{dc}} \tag{2}$$

being α_{ia}, α_{dc}, α_{ea} the gains of the instrumentation amplifier, rectifier and error amplifier, respectively, and G_m the equivalent transconductance of the current oscillator. For the condition,

$$Z_{xo}.G_m.\alpha_{ea}.\alpha_{ia}.\alpha_{dc} \gg 1 \tag{3}$$

the voltage at ZUT has the amplitude,

$$V_{xo} = \frac{V_{ref}}{\alpha_{ia}.\alpha_{dc}} \tag{4}$$

This voltage remains constant if α_{ia} and α_{dc} are also constants. Hence, the Pstat condition is fulfilled if the condition in eq. (3) is true. On the other hand, considering the relationship between the current i_x and the voltage V_m ($i_{xo}=G_m.V_m$), the impedance magnitude can be expressed as,

$$Z_{xo} = \frac{V_{xo}}{G_m.V_m} \tag{5}$$

Equation (5) means that by measuring the **magnitude voltage V_m**, the magnitude Z_{xo} can be calculated, since V_{xo} and G_m are known from eq. (4) and design parameters. For example, for a electrode with V_{xo} = 50mV and Z_{xo} = 100kΩ, the measures with G_m=0.1μS gives V_m = 50mV and i_{xo} = 5nA. If the load is divided by five, the V_m changes to 250mV and i_{xo} = 25nA.

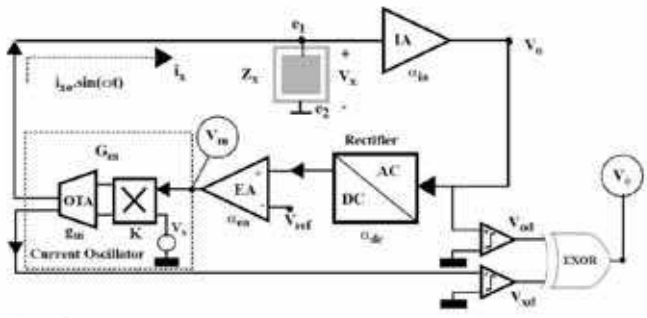

Fig. 3. Circuit blocks for impedance sensing.

For the measurement of the phase ϕ, we will consider the oscillator has an output voltage in phase with the i_x current. This signal can be squared or converted into a digital voltage signal, to be used as time reference or sync signal (V_{xd}). The V_o voltage can be also converted into a squared waveform (V_{od}) by means of a voltage comparator. If both signals feed the input of an EXOR gate, a digital signal will be obtained, the **phase voltage V_ϕ**, whose duty cycle, δ, is directly proportional to the phase of Z_x.

3.2 CMOS circuits

In the following we will give some details on the actual design considerations for CMOS circuits in Fig. 3. All circuits presented here have been designed in 0.35μm, 2P4M technology from Austria Micro-System (AMS) foundry (http://www.austriamicrosystems.com).

3.2.1 Instrumentation Amplifier

The instrumentation amplifier circuit schematic is represented in Fig. 4. It is a two-stage amplifier. A trans-conductance input stage, and a trans-resistance output stage, where filtering functionality has been included. The pass-band frequency edges were designed according to the frequency range common for impedance measurements and spectroscopy analysis. The low-pass filter corner was set at approximately 1MHz frequency, with R_2 and C_2 circuit elements, while high-pass filter corner at 100Hz, using output voltage feedback and G_{mhp} and C_1 circuit elements for its implementation. Input stage transistors have been designed to reduce the influence of electrode noise (Sawigun et al., 2006). The frequency response, magnitude and phase, are illustrated in Figures 5 (a) and (b) respectively, by using an input voltage with 10mV of amplitude.

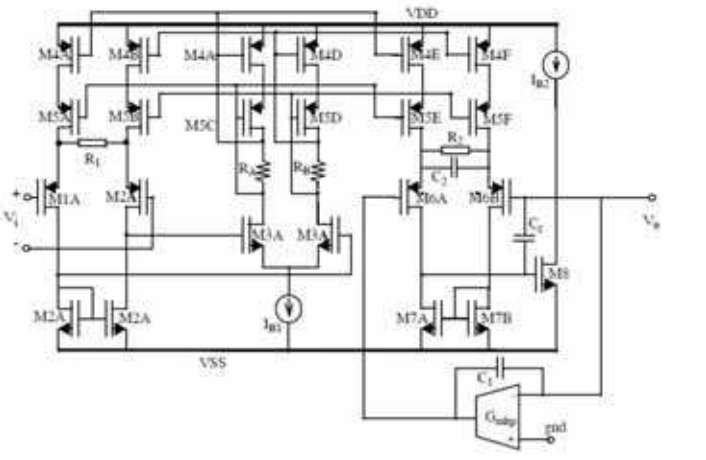

Fig. 4. Instrumentation amplifier.

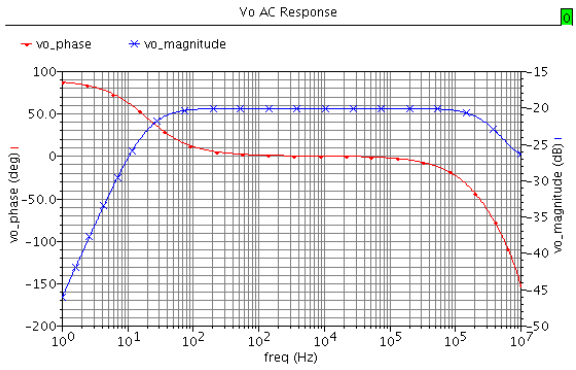

Fig. 5. Instrumentation amplifier frequency response: magnitude and phase responses for a differential input voltage of 10mV.

3.2.2 Rectifier

The full wave rectifier (positive and negative peak-detectors) in Fig. 6 is based on pass transistors (MP, MN) to load the capacitor C_r at the nearest voltage of V_o. The two comparators detect if the input signal is higher (lower) than V_{op} (V_{om}) in each instant, to charge the C_r capacitors. The discharge process of C_r is done by current sources, I_{dis}, and has been set to 1mV in a time period. Figure 7 illustrates the waveforms obtained by electrical simulations for the upper and lower rectified signals at 10 kHz. In this case, for C_r=20pF, I_{dis} has been set to 200 pA. For spectroscopy analysis, when frequency changes in a given range, the discharge current must be programmed for each frequency to fulfil the estimated 1mV voltage ripple in steady-state for the rectifier output voltage. The Comparator schematic is shown at the end of this section.

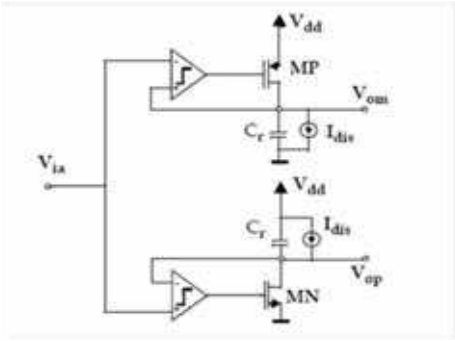

Fig. 6. Full wave rectifier schematic.

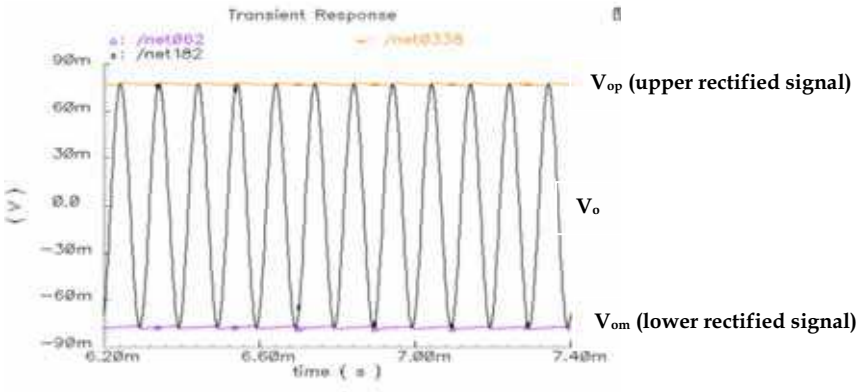

Fig. 7. Rectifier upper (V_{op}) and lower (V_{om}) output voltage waveforms. The sinusoidal signal is the Instrumentation Amplifier output voltage.

3.2.3 Error Amplifier

The first stage is a differential-to-single gain amplifier for conversion of both output voltages delivered by the full-wave rectifier. The second stage compares the result with V_{ref} and amplifies the difference to create the voltage magnitude signal, V_m, which has the information about impedance magnitude. For that, a two-stage operational amplifier is employed. One of the objectives of the system is to set at the input of the operational amplifier a voltage signal V_{dc} as near as possible to voltage V_{ref}.

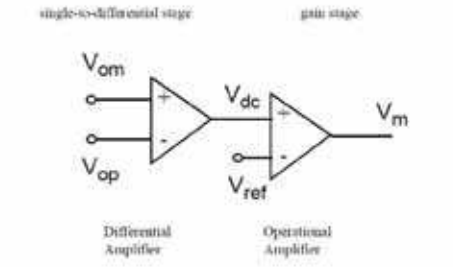

Fig. 8. Error Amplifier.

3.2.4 Current control circuit

For i_x amplitude programming, a four-quadrant multiplier and an **OTA** were designed. Both are placed in series as shown in Fig. 9. In this configuration, the external AC voltage generator is first multiplied by the voltage magnitude V_m. The result is later on converted to AC current for load excitation.

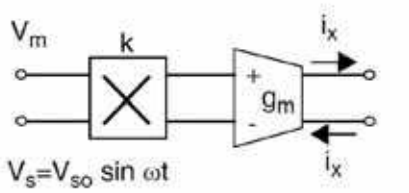

Fig. 9. The delivered AC current to electrodes (i_x) has an amplitude given by i_{xo} = (k $g_m V_{so}$).V_m, in which G_m=k$g_m V_{so}$ can be considered as the equivalent trans-conductance from V_m input voltage to i_x output current. The amplitude of i_x can be programmed with the V_m voltage.

The schematic of the multiplier circuit is shown in Fig. 10. It has two inputs that are employed for external AC voltage generator, V_s, and the voltage magnitude, V_m. The multiplier output waveforms (V_m x V_s) are shown in Fig. 11. In this figure, the AC signal V_s, has 200mV of amplitude at 10 kHz frequency, and it is multiplied by a DC signal, V_m, in the range of [0,200mV]. The differential output is given by

$$V_{out} = V_{out1} - V_{out2} = 2R\sqrt{k_n k_p}\,V_m V_s = KV_m V_s \tag{6}$$

Being K the constant of the multiplier, and k_n and k_p the trans-conductance parameter for M1 and M6 transistors.

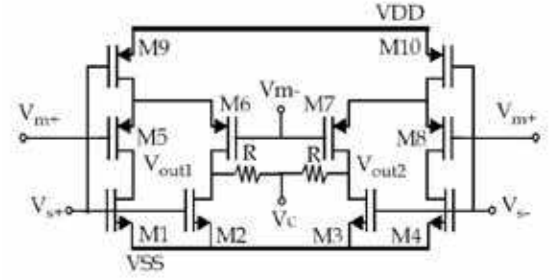

Fig. 10. Circuit schematic for the multiplier.

$$V_m \text{ x } V_s = K\, V_{so}\, V_m \sin \omega t$$

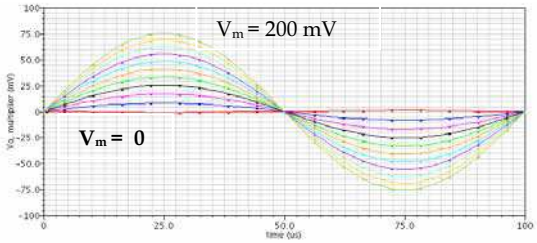

V_m [0,200mV]
V_{so} = 200 mV

Fig. 11. Waveforms for the multiplier output voltage.

The operational transconductance amplifier employed has the schematic in Fig. 12. The cascode output stage has been chosen to reduce the load effect due to large ohmic values in loads (Z_{xo}). Typical output resistances for cascode output stages are bigger than 100MΩ, so errors expected due to load resistance effects will be small.

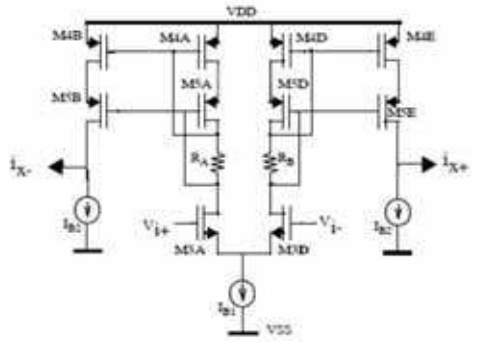

Fig. 12. Operational Transconductance Amplifier (OTA) CMOS schematic.

3.2.5 Comparator

The voltage comparator selected is shown in Fig. 13. A chain of inverters have been added at its output for fast response and regeneration of digital levels.

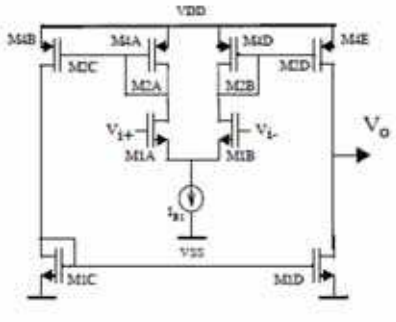

Fig. 13. Comparator schematic.

With the data employed, the voltage applied to load composed by the measurement set-up and load under test, V_x, has amplitude of 8mV. In electrode based measures, V_{xo} has typically low and limited values (tens of mV) to control its expected electrical performance (Borkholder, 1998) to secure a non-polarisable performance of the interface between an electrode and the electrolyte or biological material in contact with it. This condition can be preserved by design thanks to the voltage limitation imposed by the Pstat operation mode.

3.3 System Limitations

Due to the high gain of the loop for satisfying the condition in eq. (3), it is necessary to study the stability of the system. In steady-state operation, eventual changes produced at the load

can generate variations at the rectifier output voltage that will be amplified α_{ea} times. If ΔV_{dc} is only 1 mV, changes at the error amplifier output voltage will be large, of 500mV (for α_{ea} =500) leading to out-of-range for some circuits. To avoid this, some control mechanisms should be included in the loop. We propose to use a first order low-pass filter at the error amplifier output. This LPF circuit shown in Fig. 14 acts as a delay element, avoiding an excessively fast response in the loop, by including a dominant pole. For a given ΔV_{dc} voltage increment, the design criterium is to limit, in a time period of the AC signal, the gain of the loop below unity. This means that instantaneous changes in the error amplifier input voltage cannot be amplified with a gain bigger than one in the loop, avoiding an increasing and uncontrolled signal. The opposite will cause the system to be unstable. To define parameters in the first order filter, we analize the response of the loop to a ΔV_{dc} voltage increment. If we cut the loop between the rectifier and the error amplifier, and suppose an input voltage increment of ΔV_{dc}, the corresponding voltage response at the rectifier output will be given by the expresion,

$$\Delta V_{dc,out} = G_m.\alpha_{dc}.\alpha_{ea}.\alpha_{ia}.Z_{xo}.(1-e^{-t/\tau})\Delta V_{dc} \tag{7}$$

For a gain below unity, it should be set that, in a period of time t = T, the output voltage increment of the rectified signal is less than the corresponding input voltage changes, $\Delta V_{dc,out} < \Delta V_{dc}$, leading to the condition,

$$1 < G_m.\alpha_{dc}.\alpha_{ea}.\alpha_{ia}.Z_{xo}.(1-e^{-T/\tau}) \tag{8}$$

Which means a time constant condition given by,

$$\tau < \frac{T}{\ln(\frac{\alpha_o}{\alpha_o - 1})} \tag{9}$$

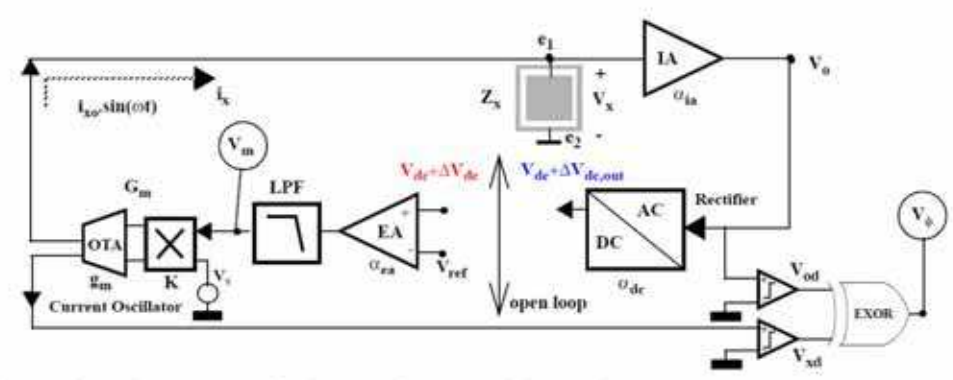

Fig. 14. Open loop system for the steady-state stability analysis.

being $\alpha_o=Z_{xo}.G_m.\alpha_{ia}.\alpha_{dc}.\alpha_{ea}$ the closed-loop gain of the system. This condition makes filter design dependent on ZUT through the paramenter Z_{xo} or impadance magnitude to be

measured. So the Z_{xo} value should be quoted in order to apply the condition in eq. (9) properly. For example, if we take α_o = 100, for a 10 kHz working frequency, the period of time is T=0.1 ms, and τ < 9.94991 ms. For a C_F = 20pF value, the corresponding R_F = 500MΩ. Preserving by design large α_o values, which are imposed by eq. (3), the operation frequency will define the values of time constant τ in LPF.

Another problem will be the start-up operation when settling a new measurement. In this situation, the reset is applied to the system by initializing to zero the filter capacitor. All measures start from V_m=0, and several periods of time are required to set its final steady-state. This is the time required to load the capacitors C_r at the rectifier up to their steady-state value. When this happens, the closed-loop gain starts to work. This can be observed at the waveforms in Fig. 15, where the settling transient for the upper-lower output voltages of the rectifier are represented. When signals find a value of 80mV, the loop starts to work. The number of periods required for the settlig process is N_c. We have taken a conservative value in the range [20,40] for N_c in the automatic measurement presented in section 6. This number depends on the charge-discarge C_r capacitor process, which during settling process is limited to a maximum of 1 mV in a signal period, since the control loop is not working yet. The N_c will define the time required to perform a measurement: T. N_c. In biological systems, time constants are low and N_c values can be selected without strong limitations. However, for massive data processing such as imaging system, where a high number of measurements must be taken to obtain a frame, an N_c value requires an optimun selection.

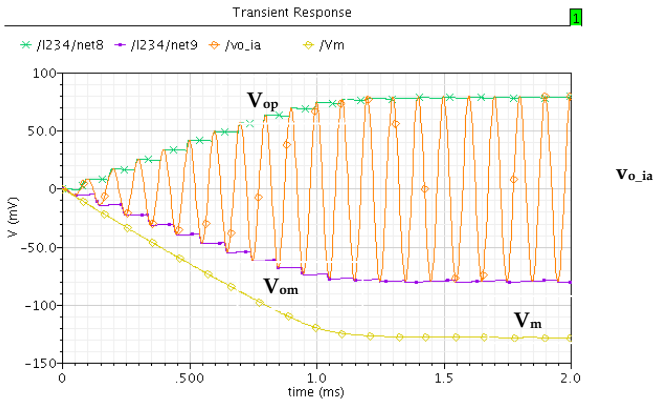

Fig. 15. Settling time transient from V_m=0 to its steady-state, V_m=-128.4mV. The upper and lower rectifier output voltages detect the increasing (deceasing) signal at the output amplifier during a settling period of about N_c=15 cycles of the AC input signal. After that, feedback loop gain starts to work, making the amplifier output voltage constant.

4. Simulation Results

4.1 Resistive and capacitive loads

Electrical simulations were performed for resistive and capacitive loads to demonstrate the correct performance of the measurement system. Initially, a 10kHz frequency was selected, and three types of loads: resistive (Z_x = 100kΩ), RC in paralell (Z_x = 100kΩ||159pF) and

capacitive (Z_x = 159pF). The system parameters were set to satisty α_o = 100, being α_{ia} = 10, α_{dc} = 0.25, α_{ea} = 500, G_m = 1.2uS, and V_{ref} = 20mV. Figure 16 shows the waveforms obtained, using the electrical simulator Spectre, for the instrumentation amplifier output voltage V_o ($\alpha_{ia}.V_x$) with the corresponding positive and negative rectified signals (V_{op} and V_{om}), the current at the load, i_x, and the signals giving the information about the measurements: magnitude voltage, V_m, and phase voltage, V_ϕ, for the three loads. The amplifier output voltage V_o is nearly constant and equal to 80mV for all loads, fulfilling the Pstat condition ($V_{xo} = V_o/\alpha_{ia}$ = 8mV), while i_x has an amplitude matched to the load. The V_m value gives the expected magnitude of Z_{xo} using eqs. (4) and (5) in all cases, as the data show in Table 1. The measurement duty-cycle allows the calculus of the Z_x phase. The 10kHz frequency has been selected because the phase shift introduced by instrumentation amplifier is close to zero, hence minimizing its influence on phase calculations. This and other deviations from ideal performance derived from process parameters variations should be adjusted by calibration. Errors in both parameters are within the expected range (less than 1%) and could be reduced by increasing the loop gain value.

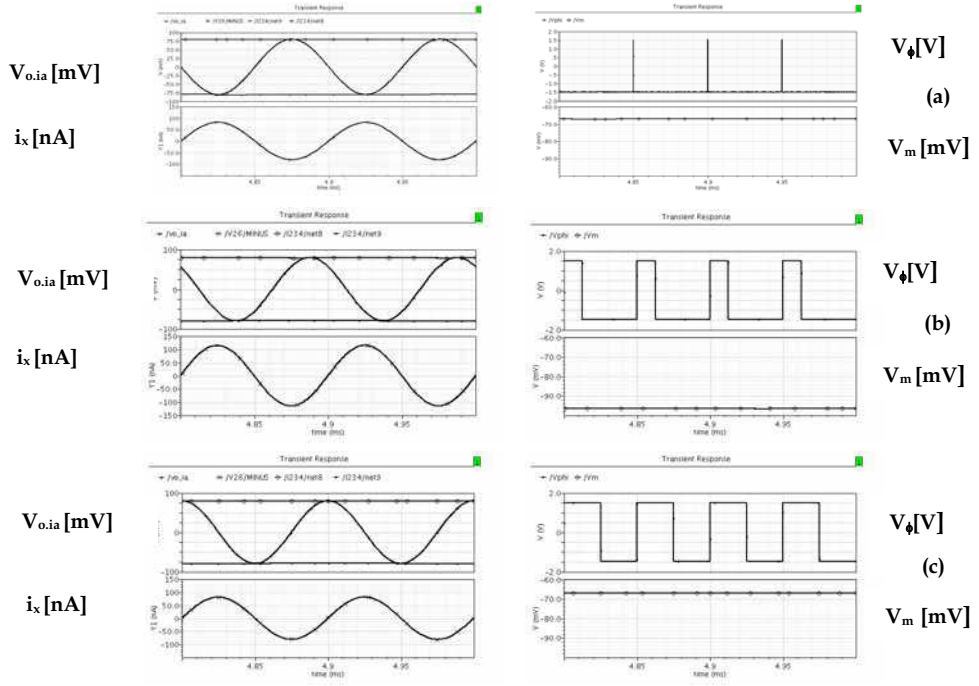

Fig. 16. Simulated waveforms for Z_x: (a) 100kΩ, (b) 100kΩ||159pF, and (c) 159pF, showing the amplifier output voltage ($V_{o,ia}$), load current (i_x), and voltages for measurements: voltage magnitude: V_m and voltage phase: V_ϕ.

Another parallel RC load has been simulated. In this case, the working frequency has been changed to 100kHz, being C_x = 15.9pF, and the values of R_x in the range [10kΩ, 1MΩ], using G_m=1.6μS. The results are listed in Table 2 and represented in Fig. 17. It could be observed an excellent match with the expected performance.

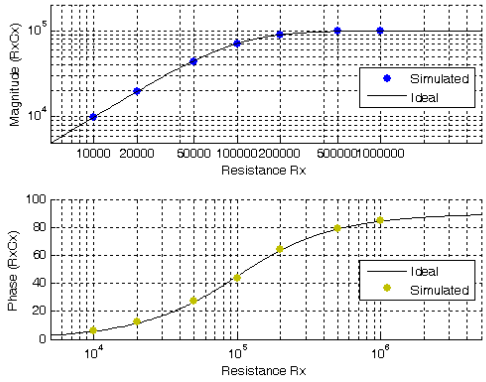

Fig. 17. Magnitude and phase for $R_x||C_x$, for C_x = 15.9pF and R_x belongs to the range [10 kΩ, 1 MΩ], at 100 kHz frequency. Dots correspond to simulated results.

Z_x	V_m [mV]	δ	Z_{xo}[kΩ]		ϕ[º]	
	sim	sim	sim	teo	sim	teo
Case R	67.15	0.005	99.28	100.0	0.93	0
Case RC	94.96	02.47	70.20	70.70	44.44	45
Case C	67.20	0.501	99.21	100.0	90.04	90

Table 1. Simulation results at 10kHz for several RC loads.

R_x [kΩ]	V_m [mV]	δ	V_{xo}[mV]	Z_{xo}[kΩ]	ϕ[º]
10	491.0	0.24	7.8	9.92	6.34
20	251.2	0.40	7.8	19.43	12.1
50	112.7	0.83	7.9	43.60	27.6
100	69.7	1.34	7.9	70.80	43.6
200	55.2	1.85	7.9	89.53	64.3
500	50.4	2.27	7.9	97.97	79.4
1000	49.7	2.42	7.9	99.35	84.8

Table 2. Simulation results for $R_x||C_x$ load. (C_x=15.9pF, f=100kHz, ϕ_{IA}(100kHz)=-2.3º, G_m=1.6uS.

5. Four-Electrode System Applications

A **four wire system** for Z_x measurements is shown in Figures 18 (a) and (b). This kind of set-up is useful in electrical impedance tomography (EIT) of a given object (Holder, 2005), decreasing the electrode impedance influence (Z_{e1}-Z_{e4}) on the output voltage (V_o) thanks to the instrumentation amplifier high input impedance. Using the same circuits described before, the electrode model in (Yúfera et al., 2005), and a 100kΩ load, the waveforms in

Fig. 19 are obtained. The voltage at Z_x load matches the amplitude of V_{xo}=8mV, and the calculus of the impedance value at 10kHz frequency (Z_{xo}=99.8kΩ and ϕ=0.2º) is correct. The same load is maintained in a wide range of frequencies (100Hz to 1MHz) achieving the magnitude and phase listed in Table 3. The main deviations are present at the amplifier bandpass frequency edges due to lower and upper -3dB frequency corners. It can be observed the phase response measured and the influence due to amplifier frequency response in Fig. 5.

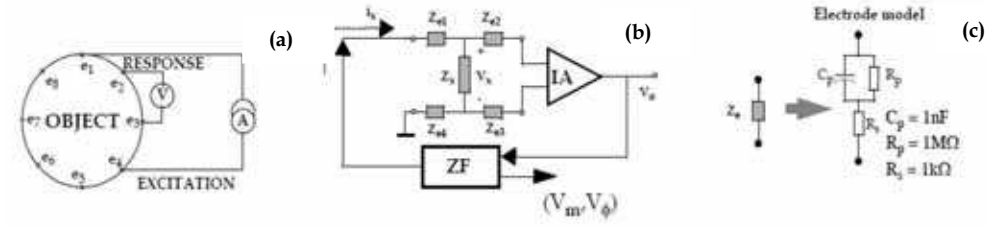

Fig. 18. (a) Eight-electrode configuration for Electrical Impedance Tomography (EIT) of an object. (b) Four-electrode system: Z_{ei} is the impedance of the electrode i. (c) Electrical model for the electrode model.

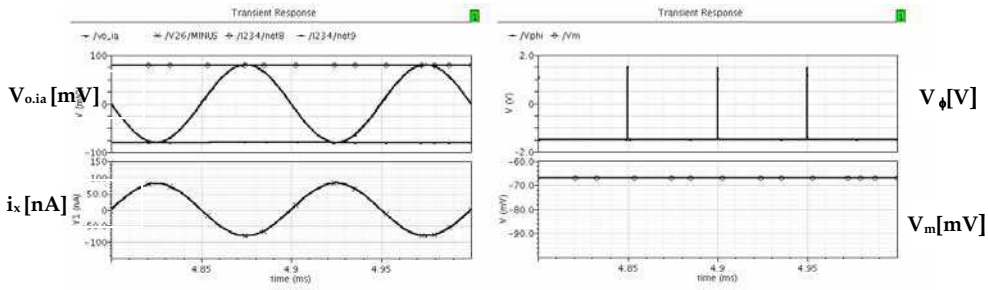

Fig. 19. Four-electrode simulation results for Z_x=100kΩ at 10 kHz frequency.

Frequency [kHz]	Z_{xo}[kΩ]		ϕ[º]	
	sim	teo	sim	teo
0.1	96.17	92.49	11.70	13.67
1	99.40	100.00	1.22	1.90
10	99.80	100.00	-0.20	-0.12
100	99.70	100.00	-4.10	-3.20
1000	95.60	96.85	-40.60	-32.32

Table 3. Simulation results for four-electrode setup and Z_x=100kΩ.

6. Two-Electrode System Applications

A two-electrode system is employed in Electric Cell substrate Impedance Spectroscopy (ECIS) (Giaever et al., 1992) as a technique capable of obtaining basic information on single or low concentration of cells (today, it is not well defined if two or four electrode systems

are better for cell impedance characterization (Bragos et al., 2007)). The main drawback of two-wire systems is that the output signal corresponds to the series of two electrodes and the load, being necessary to extract the load from the measurements (Huang et al., 2004). Figures 20 (a) and (b) show a two-electrode set-up in which the load or sample (100kΩ) has been measured in the frequency range of [100Hz,1MHz]. The circuits parameters were adapted to satisfy the condition $Z_{xo}G_m\alpha_{ia}\alpha_{dc}\alpha_{ea}=100$, since Z_{xo} will change from around 1MΩ to 100kΩ when frequency goes from tens of Hz to MHz, due to electrode impedance dependence. The simulation data obtained are shown in Table 4. At 10kHz frequency, magnitude Z_{xo} is now 107.16kΩ, because it includes two-electrodes in series. The same effect occurs for the phase, being now 17.24°. The results are in Table 4 for the frequency range considered. The phase accuracy observed is better at the mid-bandwidth.
In both cases, the equivalent circuit described in Huang (2004) has been employed for the electrode model. This circuit represents a possible and real electrical performance of electrodes in some cases. In general, the electric model for electrodes will depend on the electrode-to-sample and/or medium interface (Joye et al., 2008) and should be adjusted to each measurement test problem. In this work a real and typical electrode model has been used to validate the proposed circuits.

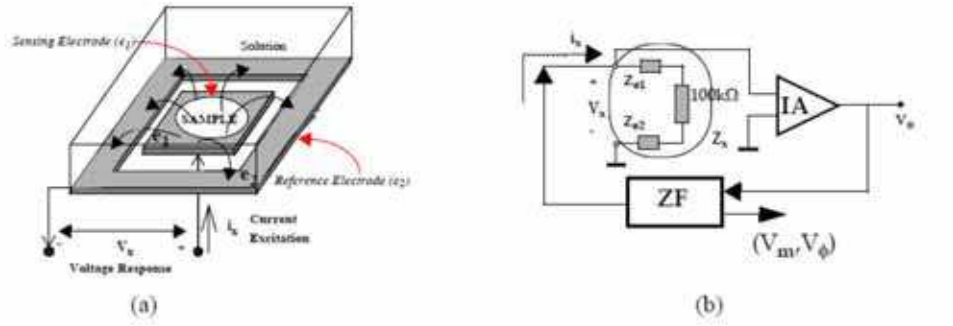

Fig. 20. (a) Two-electrode system with a sample on top of electrode 1 (e_1). (b) Equivalent circuit employed for an R_{SAMPLE}=100kΩ. Z_x includes Z_{e1}, Z_{e2} and R_{SAMPLE} resistance.

Frequency [kHz]	Z_{xo}[kΩ]		ϕ[°]	
	Sim	Teo	Sim	Teo
0.1	1058.8	1087.8	-40.21	-19.00
1	339.35	344.70	-56.00	-62.88
10	107.16	107.33	-17.24	-17.01
100	104.80	102.01	-6.48	-5.09
1000	104.24	102.00	-37.80	-32.24

Table 4. Simulation results for two-electrode set-up and Z_x=100kΩ.

6.1 Cell location applications

The cell-electrode model: An equivalent circuit for modelling the electrode-cell interface performance is a requisite for electrical characterization of the cells on top of electrodes.

Fig. 21 illustrates a two-electrode sensor useful for the ECIS technique: e_1 is called sensing electrode and e_2 reference electrode. Electrodes can be fabricated in CMOS processes using metal layers (Hassibi et al., 2006) or adding post-processing steps (Huang et al., 2004). The sample on e_1 top is a cell whose location must be detected. The circuit models developed to characterize electrode-cell interfaces (Huang, 2004) and (Joye, 2008) contain technology process information and assume, as main parameter, the overlapping area between cells and electrodes. An adequate interpretation of these models provides information about: a) *electrical simulations*: parameterized models can be used to update the actual electrode circuit in terms of its overlapping with cells. b) *imaging reconstruction*: electrical signals measured on the sensor can be associated to a given overlapping area, obtaining the actual area covered on the electrode from measurements done.

In this work, we selected the electrode-cell model reported by Huang et al. This model was obtained by using finite element method simulations of the electromagnetic fields in the cell-electrode interface, and considers that the sensing surface of e_1 could be totally or partially filled by cells. Figure 22 shows this model. For the two-electrode sensor in Fig. 21, with e_1 sensing area A, $Z(\omega)$ is the impedance by unit area of the empty electrode (without cells on top). When e_1 is partially covered by cells in a surface A_c, $Z(\omega)/(A-A_c)$ is the electrode impedance associated to non-covered area by cells, and $Z(\omega)/A_c$ is the impedance of the covered area. R_{gap} models the current flowing laterally in the electrode-cell interface, which depends on the electrode-cell distance at the interface (in the range of 10-100nm). The resistance R_s is the spreading resistance through the conductive solution. In this model, the signal path from e_1 to e_2 is divided into two parallel branches: one direct branch through the solution not covered by cells, and a second path containing the electrode area covered by the cells. For the empty electrode, the impedance model $Z(\omega)$ has been chosen as the circuit illustrated in Fig. 22(c), where C_p, R_p and R_s are dependent on both electrode and solution materials. Other cell-electrode models can be used (Joye et al., 2008), but for those the measurement method proposed here is still valid. We have considered for e_2 the model in Fig 22(a), not covered by cells. Usually, the reference electrode is common for all sensors, being its area much higher than e_1. Figure 23 represents the impedance magnitude, Z_{xoc}, for the sensor system in Fig. 21, considering that e_1 could be either empty, partially or totally covered by cells.

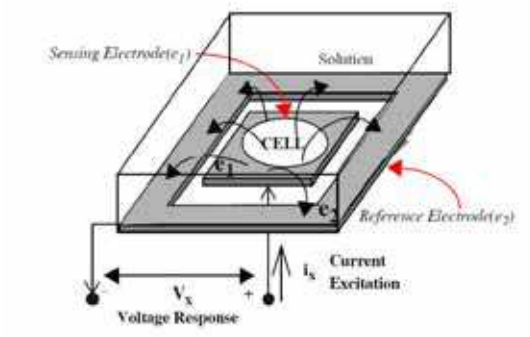

Fig. 21. Basic concept for measuring with the ECIS technique using two electrodes: e_1 or sensing electrode and e_2 or reference electrode. AC current i_x is injected between e_1 and e_2, and voltage response V_x is measured from e_1 to e_2, including effect of e_1, e_2 and sample impedances.

The parameter *ff* is called *fill factor*, being zero for A_c=0 (empty electrode), and 1 for A_c=A (full electrode). We define Z_{xoc} (*ff*=0) = Z_{xo} as the impedance magnitude of the sensor without cells.

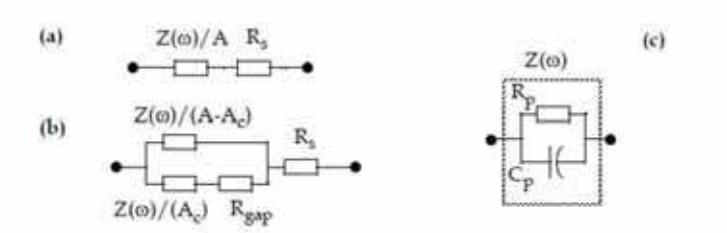

Fig. 22. Electrical models for (a) e_1 electrode without cells and, (b) e_1 cell-electrode. (c) Model for Z(ω).his work.

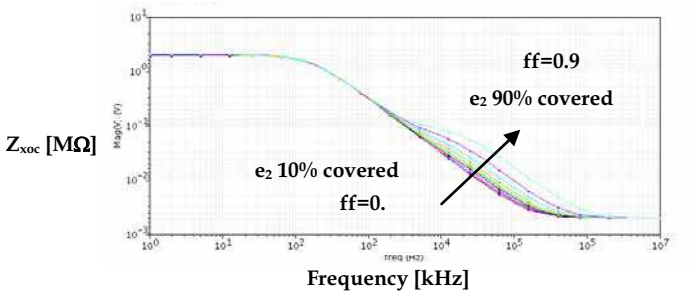

Fig. 23. Sensor impedance magnitude when the fill factor parameter (*ff*) changes. C_p=1nF, R_p=1MΩ, R_s=1kΩ and R_{gap}=100kΩ.

Absolute changes on impedance magnitude of e_1 in series with e_2 are detected in a [10 kHz, 100 kHz] frequency range as a result of sensitivity to area covered on e_1. Relative changes can inform more accurately on these variations by defining a new figure-of-merit called *r* (Huang et al., 2004), or *normalized impedance magnitude*, by the equation,

$$r = \frac{Z_{xoc} - Z_{xo}}{Z_{xo}} \tag{10}$$

Where *r* represents the relative increment of the impedance magnitude of two-electrode system with cells (Z_{xoc}) relative to the two-electrode system without them (Z_{xo}). The graphics of *r* versus frequency is plotted in Fig. 24, for a cell-to-electrode coverage *ff* from 0.1 to 0.9 in steps of 0.1. We can identify again the frequency range where the sensitivity to cells is high, represented by *r* increments. For a given frequency, each value of the normalized impedance *r* can be linked with its *ff*, being possible to detect the cells and to estimate the sensing electrode covered area, A_c. For imaging reconstruction, this work proposes a new CMOS

system to measure the *r* parameter for a given frequency, and detect the corresponding covering area on each electrode according to sensitivity in Fig 24.

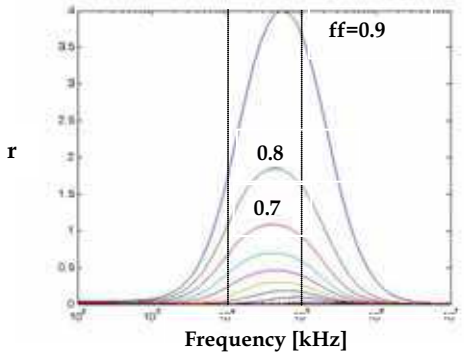

Fig. 24. Normalized magnitude impedance *r* for *ff*= 0.1 to 0.9 in steps of 0.1**.**

6.2 2D image applications

To test the proposed method for impedance sensing, we have chosen a simulation case with an 8x8 two-electrode array. The sample input to be analysed is a low density MCF-7 epithelial breast cancer cell culture shown in Fig. 25(a). In this image some areas are covered by cells and others are empty. Our objective is to use the area parametrized electrode-cell model and the proposed circuits to detect their location. The selected pixel size is 50μm x 50μm, similar to cell dimensions. Figure 25(a) shows the grid selected and its overlap with the image. We associate a squared impedance sensor, similar to the one described in Fig. 21, to each pixel in Fig. 25(a) to obtain a 2D system description valid for electrical simulations. An optimum pixel size can be obtained by using design curves for normalized impedance *r* and its frequency dependence. Each electrical circuit associated to each e_1 electrode in the array was initialized with its corresponding fill factor (*ff*). The matrix in Fig 25(b) is obtained in this way. Each electrode or pixel is associated to a number in the range [0,1] (*ff*) depending on its overlap with cells on top. These numbers were calculated with an accuracy of 0.05 from the image in Fig.25(a). The *ff* matrix represents the input of our system to be simulated. Electrical simulations of the full system were performed at 10kHz (midband of the IA) to obtain the value of the voltage magnitude V_m in eq. (4) for all electrodes. Pixels are simulated by rows, starting from the leftmost bottom (pixel 1) to the right-most top (pixel 64). When measuring each pixel, the voltage V_m is reset to zero and then 25 cycles (N_c) are reserved to find its steady-state, where V_m value becomes constant and is acquired. The waveforms obtained for the amplifier output voltage $\alpha_{ia}V_x$, voltage magnitude, V_m, and excitation current i_x are represented in Fig. 26. It is observed that the voltage at the sensor, V_x, has always the same amplitude (8mV), while the current decreases with *ff*. The V_m signal converges towards a DC value, inversely proportional to the impedance magnitude. Steady-state values of V_m are represented in Fig. 27 for all pixels. These are used to calculate their normalized impedances *r* using eqs. (10) and (5).

To have a graphical 2D image of the fill factor (area covered by cells) in all pixels, Fig. 28 represents the 8x8 *ff*-maps, in which each pixel has a grey level depending on its fill factor value (white is empty and black full). In particular, Fig. 28(a) represents the *ff*-map for the input image in Fig. 25(b). Considering the parameterized curves in Fig. 24 at 10kHz

frequency, the fill factor parameter has been calculated for each electrode, using the V_m simulated data from Fig. 26 and the results are represented in Fig. 28(b). The same simulations have been performed at 100kHz, obtaining the *ff*-map in Fig. 28(c). As Fig. 24 predicts, the best match with the input is found at 100kHz since normalized impedance is more sensitive and the sensor has a higher dynamic range at 100kHz than at 10kHz. In both cases, the errors obtained in the *ff* values are below 1%, therefore matching with the input is excellent. The total time required to acquired data for a full image or frame will depend on the measuring frequency, the number of cycles reserved for each pixel (N_c=25 for reported example) and the array dimension (8x8). For reported simulations 160ms and 16ms for frame, working at 10kHz and 100kHz, respectively, are required. This frame acquisition time is enough for real time monitoring of cell culture systems.

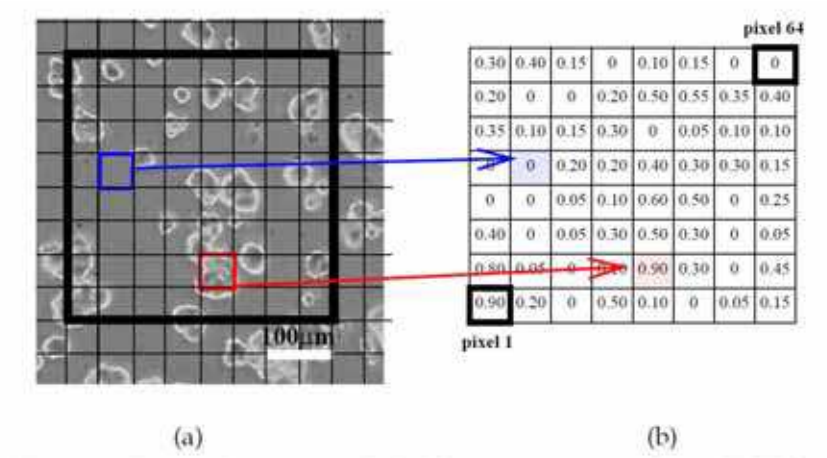

Fig. 25. (a) 8x8 pixel area selection in epithelial breast cancer cell culture. (b) Fill factor map (*ff*) associated to each electrode (pixel).

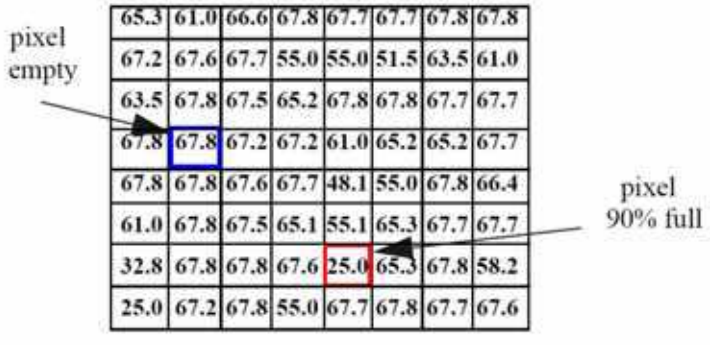

Fig. 26. 2D matrix of values for V_m [mV] in steady-state obtained from electrical simulations at 10 kHz frequency.

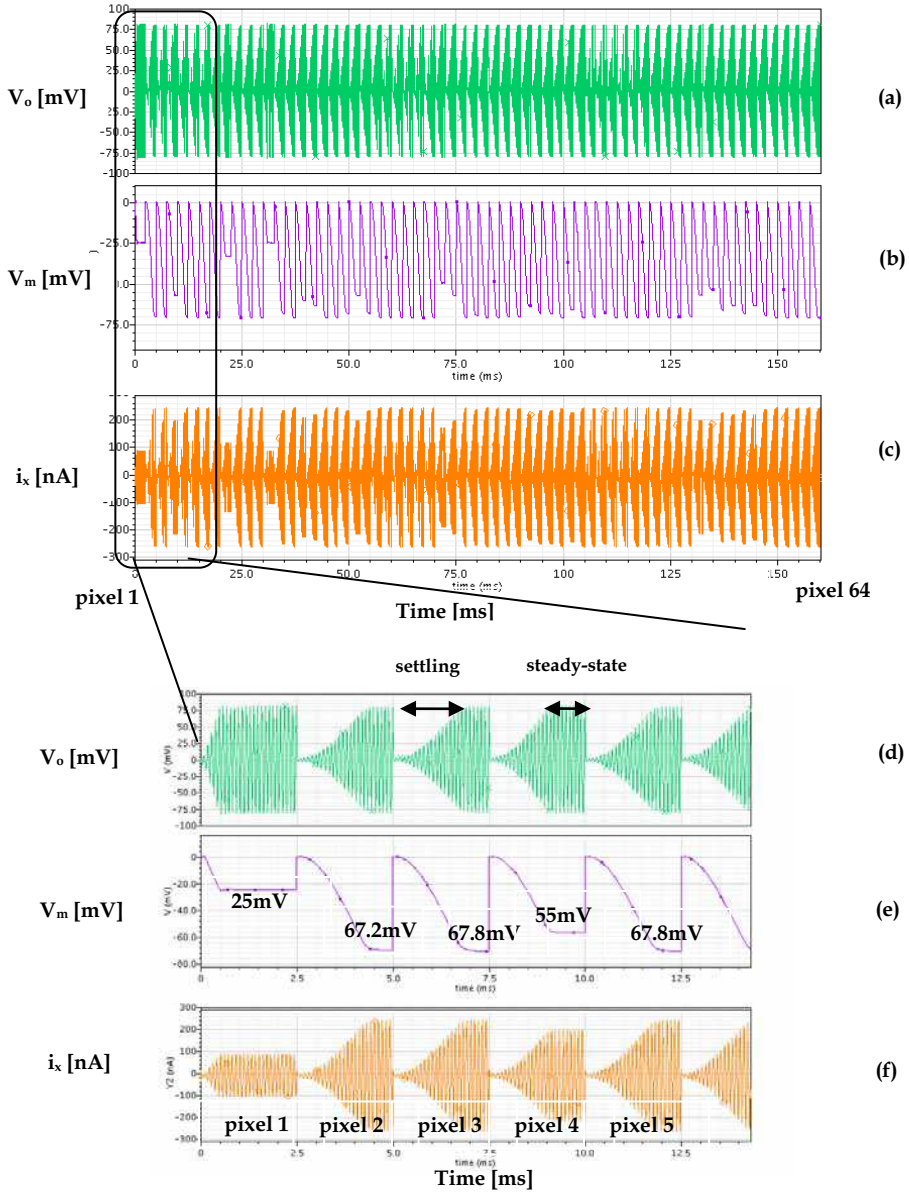

Fig. 27. Simulated waveforms for (a) $\alpha_{ia}V_x = 10V_x$, (b) V_m and (c) i_x signals for the 64 electrodes at 10 kHz. (d-f) Zoom for the first five pixels of (a-c) waveforms.

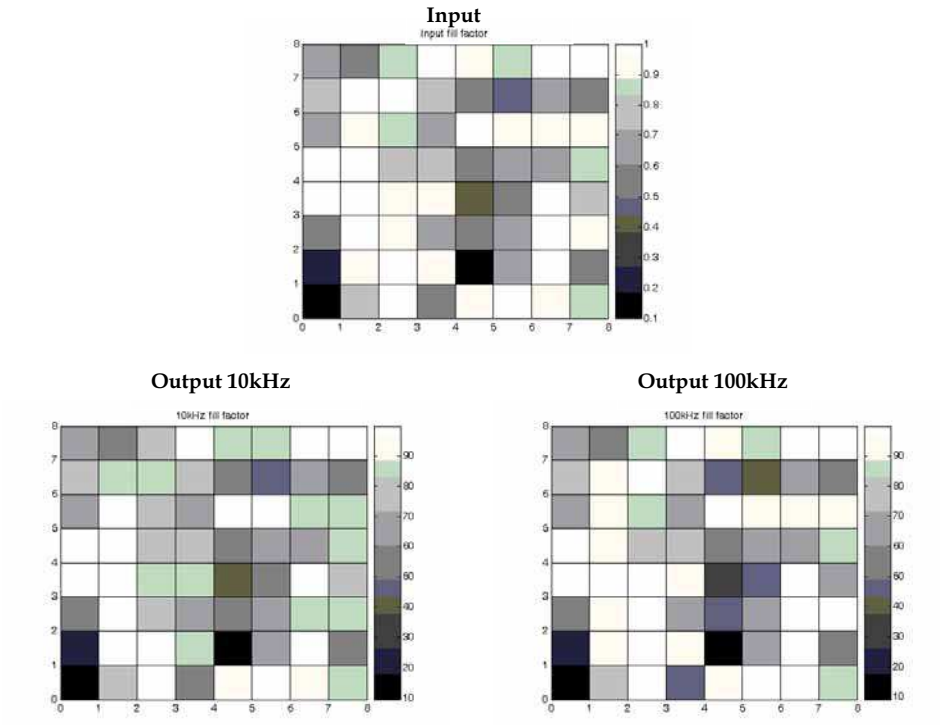

Fig. 28. 2D diagram of the fill factor maps for 8x8 pixels: (a) ideal input. Image reconstructed from simulations at (b) 10 kHz and (c) 100 kHz.

7. Conclusions

This work reports novel front-end circuits for impedance measurement based on a proposed closed-loop configuration. The system has been developed on the basis of applying an AC voltage with constant amplitude to the load under test. As a result, the proposed technique allows to perform excitation and read-out functionalities by the same circuits, delivering magnitude and phase impedance in two independent signals, easy to acquired: a constant DC signal and a digital signal with variable duty-cycle, respectively.

The proposed CMOS circuits to implement the system have been correctly validated by electrical simulation taking into account several types of resistive and capacitive loads, working at different frequencies.

A number of biomedical applications relying on impedance detection and monitoring can benefit from our proposed CBIM system in several ways: the necessity of taking/performing measurements using electrodes proves the usefulness of the proposed system because there is the possibility of limiting the voltage amplitude on the electrodes, biasing a given electrode-solution interface at the non-polarizable region, optimum for neural signal recording, for example. Also, the possibility of the simultaneous

implementation of an electrode sensor and CMOS circuits in the same substrate enables the realization of fully integrated system or lab-on-chips (LoC). This fact should be tested in future works.

Standard two- and four-electrode based systems have been tested to demostrate the feasibility of the proposed system. The results for the four-wire set-up are accurate in all the frequency band, except at the corner bandwidth of the instrumentation amplifier, where its magnitude and phase responses are the main error sources. Electrical Impedance Tomography is an excellent candidate to employ the proposed impedance measurement system.

The application of CBIM to a two-wire set-up enables the proposed system for impedance sensing of biological samples to be useful for 2D imaging. An electrical model based on the overlapping area is employed in both system simulation and image reconstruction for electrode-cell characterization, allowing the incorporation of the electrode design process on the full system specifications. Electrical simulations have been done to reproduce the ECIS technique, giving promising results in cell location and imaging, and enabling our system for other real-time applications such as cell index monitoring, cell tracking, etc. In future works, precise cell electrode model, optimized sensing circuits and design trade-off for electrode sizing will be further explored for a real experimental imaging system.

8. Acknowledgements

This work is in part supported by the Spanish founded Project: TEC2007-68072/ TECATE, *Técnicas para mejorar la calidad del test y las prestaciones del diseño en tecnologías CMOS submicrométricas*.

9. References

Ackmann, J. (1993). Complex Bioelectric Impedance Measurement System for the Frequency Range from 5Hz to 1MHz. *Annals of Biomedical Engineering*, Vol. 21, pp. 135-146

Beach, R. D. et al., (2005). Towards a Miniature In Vivo Telemetry Monitoring System Dynamically Configurable as a Potentiostat or Galvanostat for Two- and Three-Electrode Biosensors. *IEEE Transactions on Instrumentation and Measurement*, Vol. 54, No. 1, pp. 61-72

Yúfera, A. et al., (2005). A Tissue Impedance Measurement Chip for Myocardial Ischemia Detection. *IEEE Transaction on Circuits and Systems: Part I. Regular papers*, Vol. 52, No. 12, pp. 2620-2628

Huang, X. (2004). Impedance-Based Biosensor Arrays. *PhD. Thesis*, Carnagie Mellon University

Radke, S. M. et al., (2004). Design and Fabrication of a Micro-impedance Biosensor for Bacterial Detection. *IEEE Sensor Journal*, Vol. 4, No. 4, pp. 434-440

Borkholder, D. A. (1998). Cell-Based Biosensors Using Microelectrodes. *PhD Thesis*, Stanford University

Giaever, I. et al., (1996). Use of Electric Fields to Monitor the Dynamical Aspect of Cell Behaviour in Tissue Culture. *IEEE Transaction on Biomedical Engineering*, Vol. BME-33, No. 2, pp. 242-247

Holder, D. (2005). Electrical Impedance Tomography: Methods, History and Applications, Philadelphia: IOP

Pallás-Areny, R. and Webster, J. G. (1993). Bioelectric Impedance Measurements Using Synchronous Sampling. *IEEE Transaction on Biomedical Engineering*, Vol. 40, No. 8, pp: 824-829. Aug

Zhao, Y. et al., (2006). A CMOS Instrumentation Amplifier for Wideband Bio-impedance Spectroscopy Systems. *Proceedings of the International Symposium on Circuits and Systems*, pp. 5079-5082

Ahmadi, H. et al., (2005). A Full CMOS Voltage Regulating Circuit for Bio-implantable Applications. *Proceeding of the International Symposium on Circuits and Systems*, pp. 988-991

Hassibi, A. et al., (2006). A Programmable 0.18μm CMOS Electrochemical Sensor Microarray for Bio-molecular Detection. *IEEE Sensor Journal*, Vol. 6, No. 6, pp. 1380-1388

Yúfera, A. and Rueda, A. (2008). A Method for Bio-impedance Measure with Four- and Two-Electrode Sensor Systems. *30th Annual International IEEE EMBS Conference*, Vancouver, Canada, pp. 2318-2321

Sawigun, C. and Demosthenous, A. (2006). Compact low-voltage CMOS four-quadrant analogue multiplier. *Electronics Letters*, Vol. 42, No. 20, pp. 1149-1150

Huang, X., Nguyem, D., Greve, D. W. and Domach, M. M. (2004). Simulation of Microelectrode Impedance Changes Due to Cell Growth. *IEEE Sensors Journal*, Vol. 4, No 5, pp. 576-583

Yúfera, A. and Rueda, A. (2009). A CMOS Bio-Impedance Measurement System. *12th IEEE Design and Diagnostic of Electronics Circuits and Systems*, Liberec, Czech Republic, pp. 252-257

Romani, A. et al., (2004). Capacitive Sensor Array for Location of Bio-particles in CMOS Lab-on-a-Chip. *International Solid Stated Circuits Conference (ISSCC)*, 12.4

Medoro, G. et al., (2003). A Lab-on-a-Chip for Cell Detection and Manipulation. *IEEE Sensor Journ*al, Vol. 3, No. 3, pp: 317-325

Manaresi, N. et al (2003). A CMOS Chip for individual Cell Manipulation and Detection. *IEEE Journal of Solid Stated Circuits*, Vol. 38, No. 12, pp: 2297-2305. Dec

Joye, N. et al (2008). An Electrical Model of the Cell-Electrode Interface for High-Density Microelectrode Arrays. *30th Annual International IEEE EMBS Conference*, pp: 559-562

Bragos, R. et al., (2006). Four *Versus* Two-Electrode Measurement Strategies for Cell Growing and Differentiation Monitoring Using Electrical Impedance Spectroscopy. *28th Annual International IEEE EMBS Conference*, pp: 2106-2109

New Developments in Biomedical Engineering

Edited by Domenico Campolo

ISBN 978-953-7619-57-2
Hard cover, 714 pages
Publisher InTech
Published online 01, January, 2010
Published in print edition January, 2010

Biomedical Engineering is a highly interdisciplinary and well established discipline spanning across engineering, medicine and biology. A single definition of Biomedical Engineering is hardly unanimously accepted but it is often easier to identify what activities are included in it. This volume collects works on recent advances in Biomedical Engineering and provides a bird-view on a very broad field, ranging from purely theoretical frameworks to clinical applications and from diagnosis to treatment.

How to reference

In order to correctly reference this scholarly work, feel free to copy and paste the following:

Alberto Yufera and Adoracion Rueda (2010). A Closed-Loop Method for Bio-Impedance Measurement with Application to Four and Two-Electrode Sensor Systems, New Developments in Biomedical Engineering, Domenico Campolo (Ed.), ISBN: 978-953-7619-57-2, InTech, Available from: http://www.intechopen.com/books/new-developments-in-biomedical-engineering/a-closed-loop-method-for-bio-impedance-measurement-with-application-to-four-and-two-electrode-sensor

INTECH
open science | open minds

InTech Europe
University Campus STeP Ri
Slavka Krautzeka 83/A
51000 Rijeka, Croatia
Phone: +385 (51) 770 447
Fax: +385 (51) 686 166
www.intechopen.com

InTech China
Unit 405, Office Block, Hotel Equatorial Shanghai
No.65, Yan An Road (West), Shanghai, 200040, China
中国上海市延安西路65号上海国际贵都大饭店办公楼405单元
Phone: +86-21-62489820
Fax: +86-21-62489821